Science Advances
AAAS

Supplementary Materials for

Zika virus noncoding RNA cooperates with the viral protein NS5 to inhibit STAT1 phosphorylation and facilitate viral pathogenesis

Andrii Slonchak *et al.*

Corresponding author: Alexander A. Khromykh, a.khromykh@uq.edu.au; Andrii Slonchak, a.slonchak@uq.edu.au

Sci. Adv. **8**, eadd8095 (2022)
DOI: 10.1126/sciadv.add8095

The PDF file includes:

Figs. S1 to S12
Legends for tables S1 to S12

Other Supplementary Material for this manuscript includes the following:

Tables S1 to S12

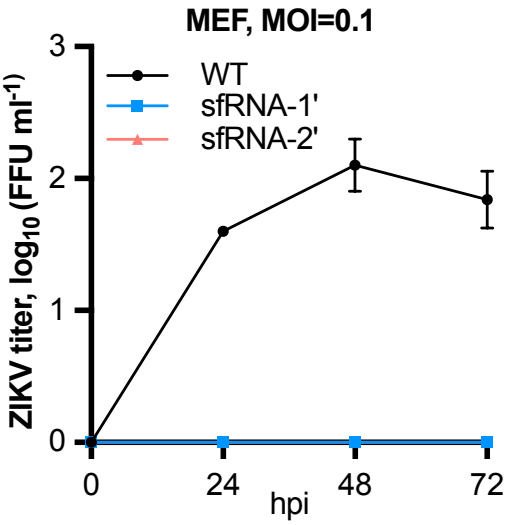

Fig. S1.

Replication of WT ZIKV and sfRNA-deficient mutant viruses in mouse embryonic fibroblasts. ZIKV titers were determined in culture fluids of mouse embryonic fibroblasts (MEF) infected at MOI=0.1. Values are the means from three independent experiments +SD.

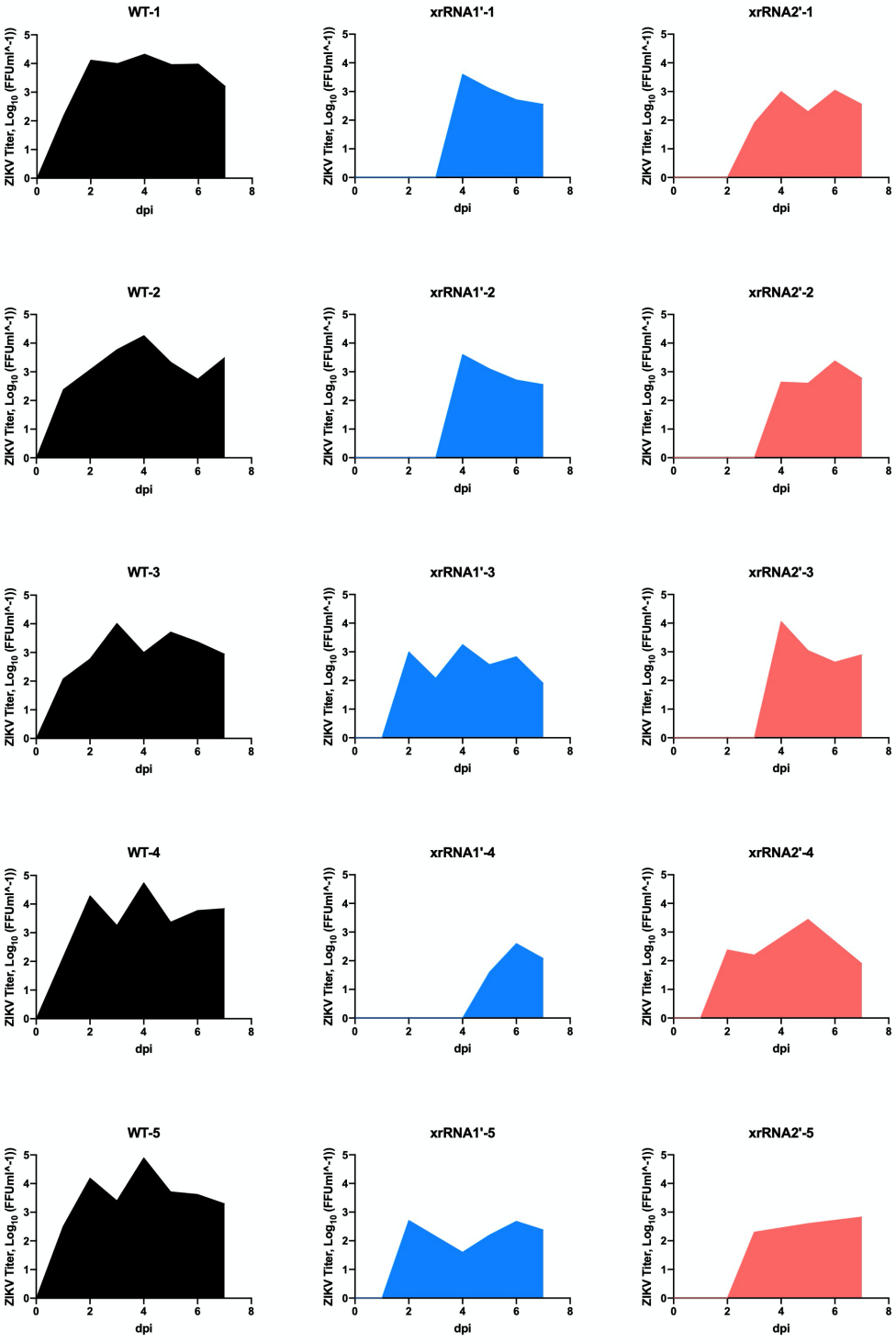

Fig. S2.

Blood viremia in AG129 mice infected with WT and sfRNA-deficient ZIKV. Mice were inoculated with 10^4 FFU of the viruses by subcutaneous injection, and blood was sampled daily for 7 days via tail bleed. Virus load kinetics for individual animals is shown, and areas under the curves are shaded.

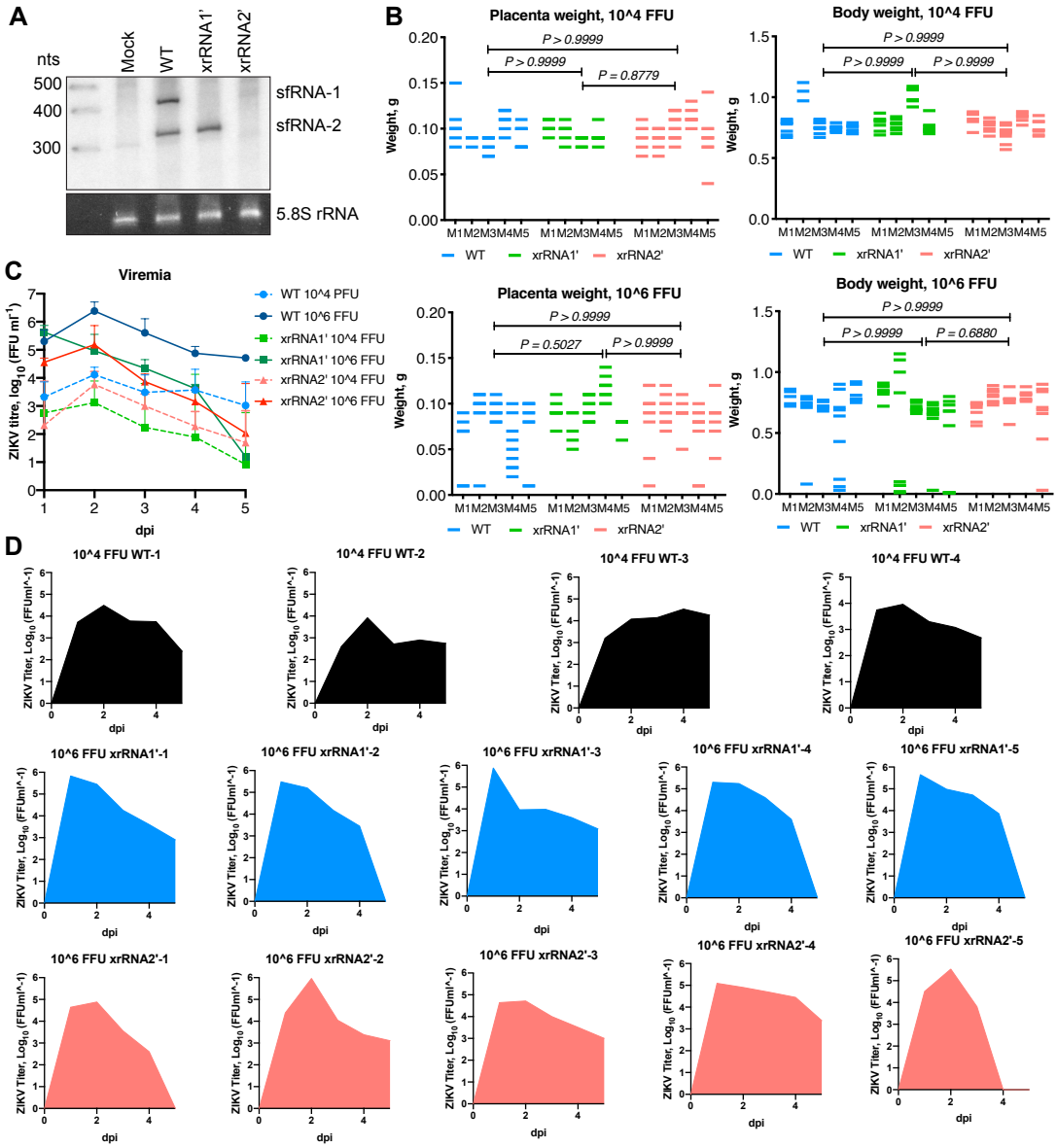

Fig. S3.

Analysis of WT and sfRNA-deficient ZIKV in mouse pregnancy model. (A) Production of sfRNA by WT virus and sfRNA-deficient mutants of $ZIKV_{Natal}$. Vero cells were infected at MOI=1, RNA was isolated at 72hpi and used for Northern blotting with a probe complementary to the most terminal 31nt of the viral genome. Bottom panel shows 5.8S rRNA visualised by Et-Br staining as a loading control. **(B)** Weight of placentas and fetuses obtained from mice infected with WT and sfRNA-deficient $ZIKV_{Natal}$ viruses. Pregnant IFNAR-/- mice were inoculated with indicated doses of WT or sfRNA-deficient ZIKVNatal viruses via subcutaneous injection, and fetal material was collected at 5 dpi. Statistical comparison of virus titres was performed by Kruskal-Wallis test with Dunn's correction. **(C)** Blood viremia in pregnant mice infected with two different doses of WT and sfRNA-deficient ZIKV mutants. **(D)** Blood viremia in IFNAR-/- mice infected with 10^4 FFU of WT ZIKV and 10^6 FFU of sfRNA-deficient mutants. Blood was sampled daily via tail bleed. Viremia in individual animals is shown, and areas under the curves are shaded.

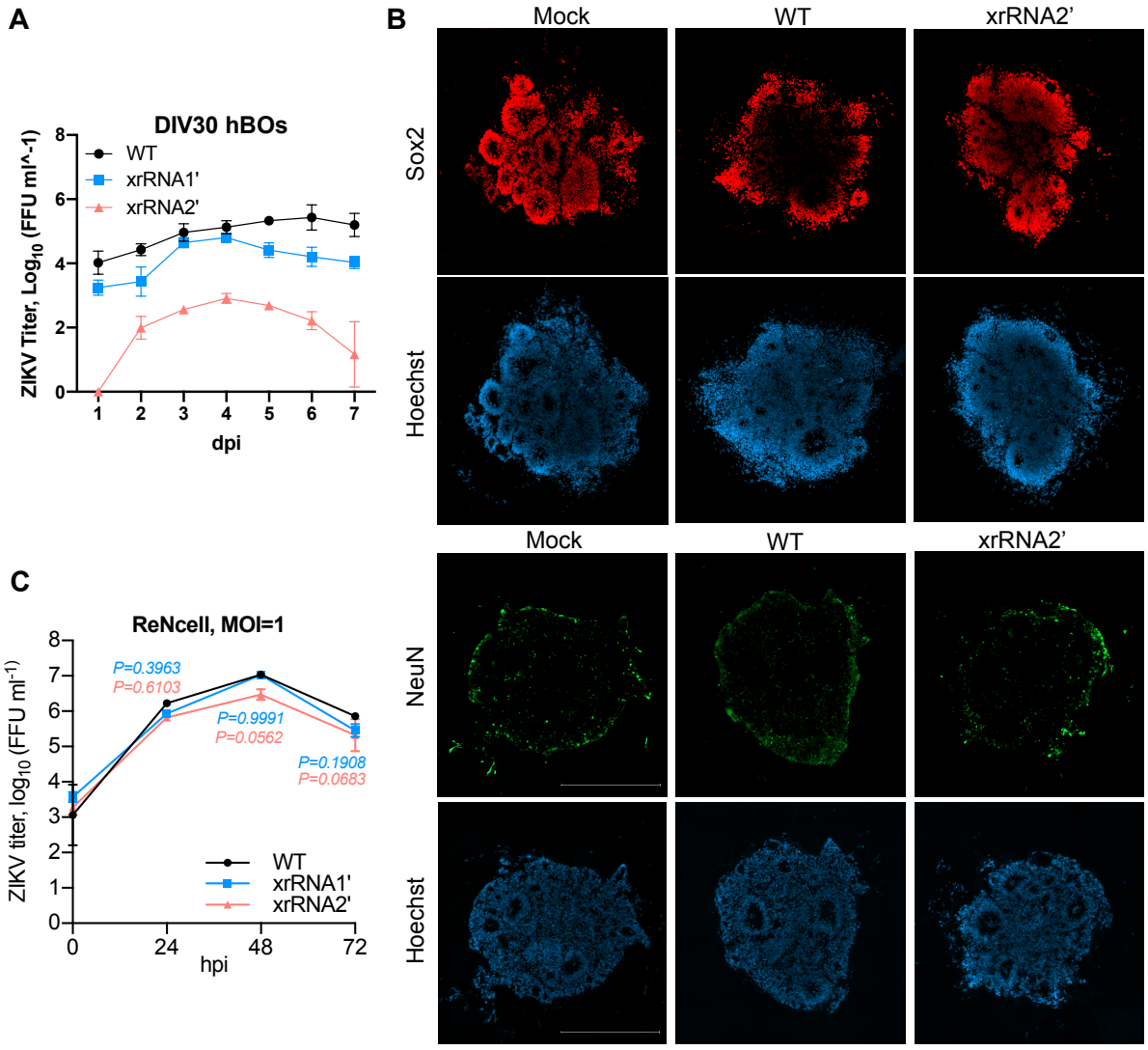

Fig. S4.
Characterization of human cerebral organoids infected with WT and sfRNA-deficient ZIKV. (A) Replication of WT ZIKV and sfRNA-deficient mutant viruses in human cerebral organoids at DIV30. Organoids were infected with 10^4 FFU of each virus, and culture fluids were sampled daily. Viral titers were determined by foci-forming assay on C6/36 cells. The values are the means from three independent experiments ±SD**. (B)** Individual channels showing immunofluorescent staining for neural progenitor marker Sox2 and nuclei (Hoechst) for the images displayed in figure 3A. Human brain organoids at DIV15 were inoculated with 10^4 FFU of WT of sfRNA-deficient ZIKV and fixed for staining at 3 dpi. The images are representative of three independent experiments, each containing 5 individual organoids per group. All experiments showed similar results. **(C)** ReNcell human neural progenitor cells were infected at MOI=1, culture fluid samples were collected at the indicated time points, and virus titers were determined by foci-forming assay. Values are the means from three biological replicates ±SD. Statistical analysis was performed by one-way ANOVA with Dunnett correction.

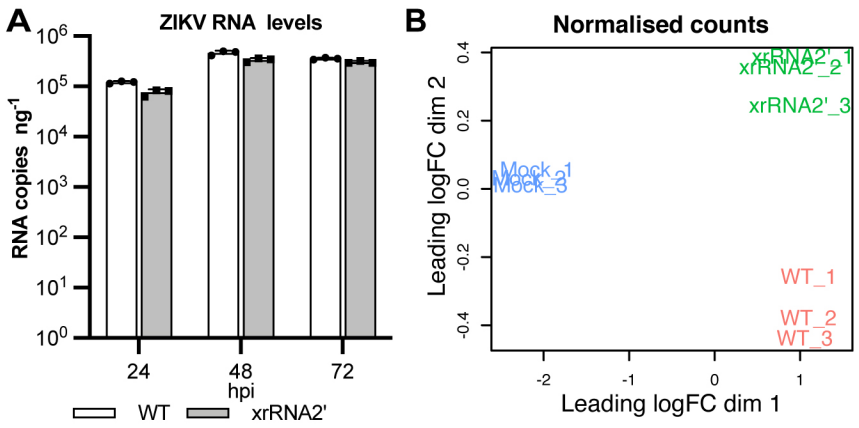

Fig. S5.

Analysis of human placental cells BeWo infected with WT and sfRNA-deficient ZIKV. (A) Viral RNA copy numbers in BeWo cells infected with WT and xrRNA2' ZIKV. ZIKV RNA was quantified by qRT-PCR using a standard curve method and normalised to the amount of input total RNA. The values are the means of three biological replicates ±SD. **(B)** Principal component analysis of RNA-Seq counts from BeWo cells infected with WT and xrRNA2' ZIKV and mock-infected cells. Count numbers were normalised to the library sizes.

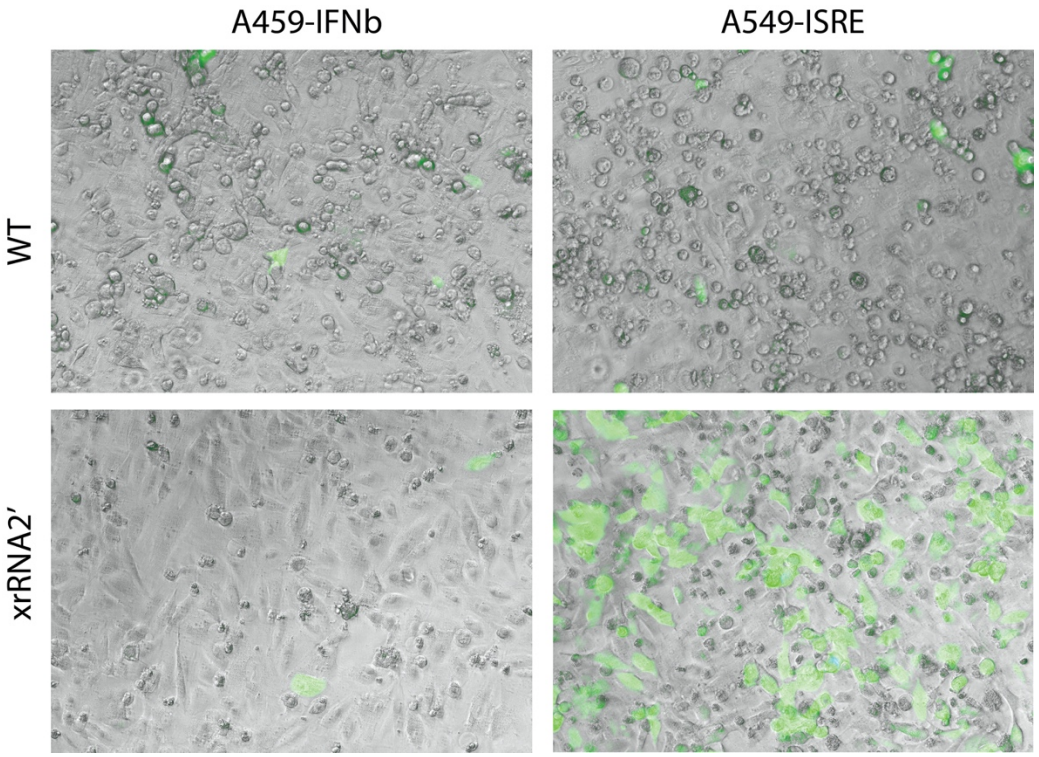

Fig. S6.
Effect of ZIKV sfRNA on the activity of IFNb and ISRE promoters. IFNb-GFP and ISRE-GFP reporter A549 cells were infected with WT or sfRNA-deficient ZIKV at MOI=0.1, and GFP fluorescence was documented at 24 hpi. The images are merged bright-field and epi-fluorescent microphotographs of live cells and are representative of three experiments that showed similar results.

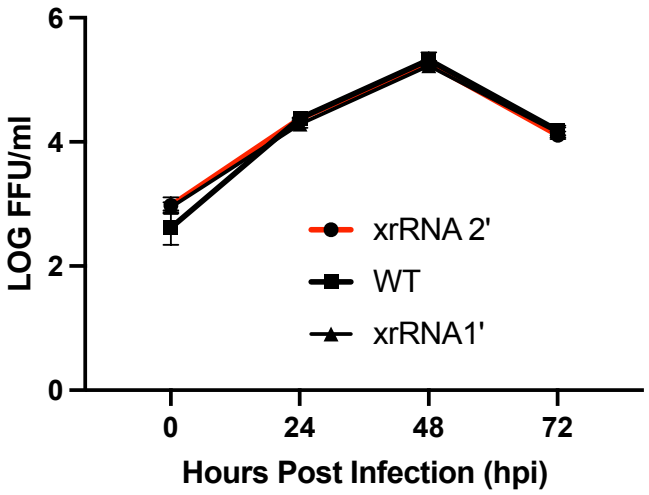

Fig. S7.

Replication of WT and sfRNA-deficient ZIKV in human placental cells HTR8 infected at high MOI. Cells were infected at MOI=5, and titers were determined by foci-forming assay on C6/36 cells. The values are the means from three independent experiments, and the error bars indicate SD.

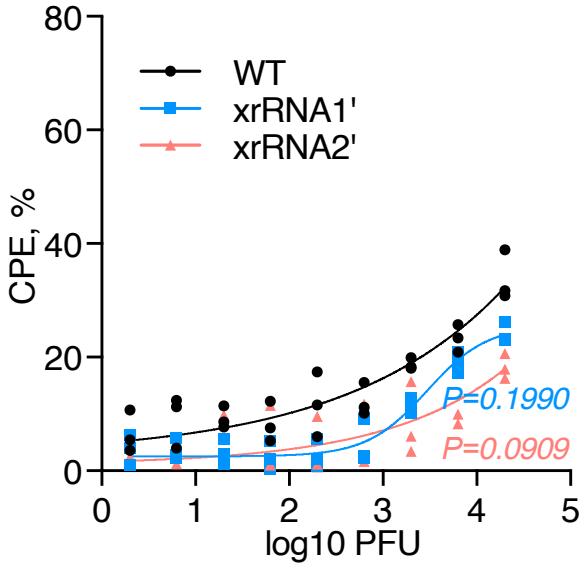

Fig. S8.

Cytotoxicity of WT and sfRNA-deficient ZIKV mutants in STAT1-deficient cells. U3A cells were infected at the indicated MOIs, and CPE was measured at 72hpi. %CPE is calculated with reference to uninfected cells grown for the same period. Statistical analysis was performed using Student's t-test, and individual values are shown.

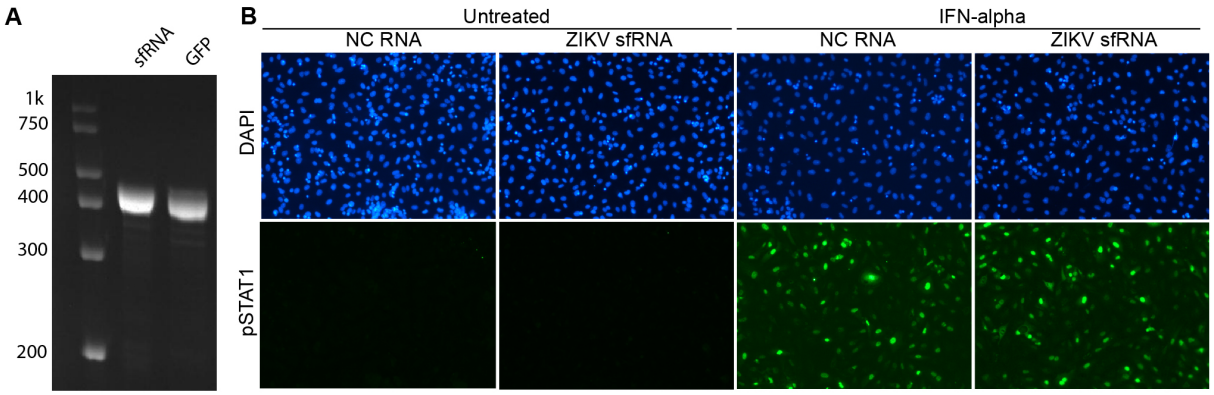

Fig. S9.

Transfected ZIKV sfRNA does not inhibit IFNα-induced phosphorylation and nuclear translocation of STAT1. (A) ZIKV sfRNA and GFP RNA produced by *in vitro* transcription visualised in Et-Br-stained polyacrylamide gel. **(B)** Immunofluorescent detection of Tyr701-phosphorylated STAT1 in Vero cells transfected with *in vitro* generated RNA and treated with IFNα1. Cells were transfected with 500ng of ZIKV 5'P-sfRNA or control 5'P-GFP RNA (NC RNA) and treated with IFNα1 at 24 hpt for 20 min. DAPI counterstaining indicates the total number of cells in the field of view.

Fig. S10.

Schematics of the constructs used for *in vitro* transcription of tagged sfRNA and control RNA. Restriction sites used for linearisation of the plasmids are indicated; T7 – T7 promoter, s1m – optimised streptavidin-binding aptamer (tag).

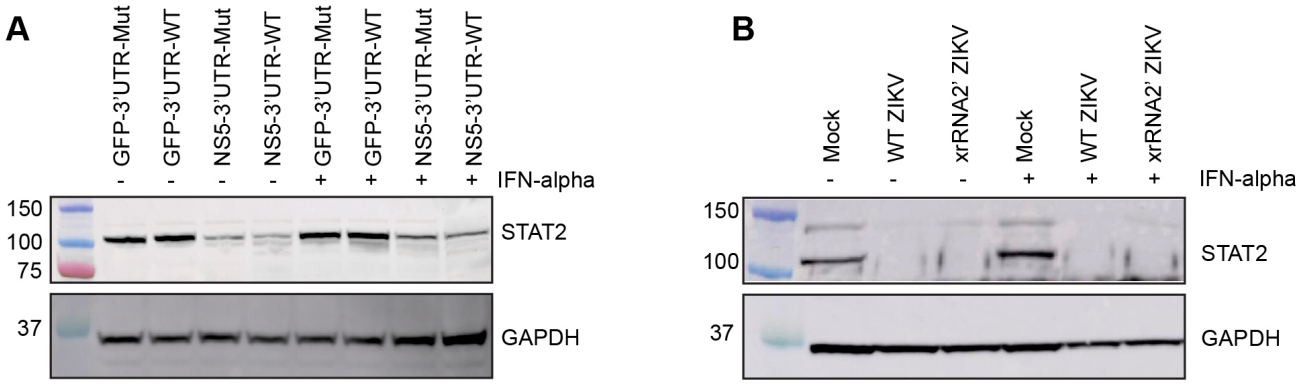

Fig. S11.

Production of ZIKV sfRNA does not affect NS5-dependent degradation of STAT2. (A) Western-blot detection of total STAT2 in HEK293 cells transfected with expression constructs (from Fig 6B) and treated with IFNα. IFN-treatment was performed at 48hpt, and cells were lysed for Western blotting after 15 min of treatment. GAPDH is shown as a loading control. **(B)** Western-blot detection of total STAT2 in Vero cells infected with WT and xrRNA2' mutant ZIKV. Cells were infected at MOI=5, and assays were performed at 48hpi. Levels of GAPDH in (A, B) are shown as a loading control.

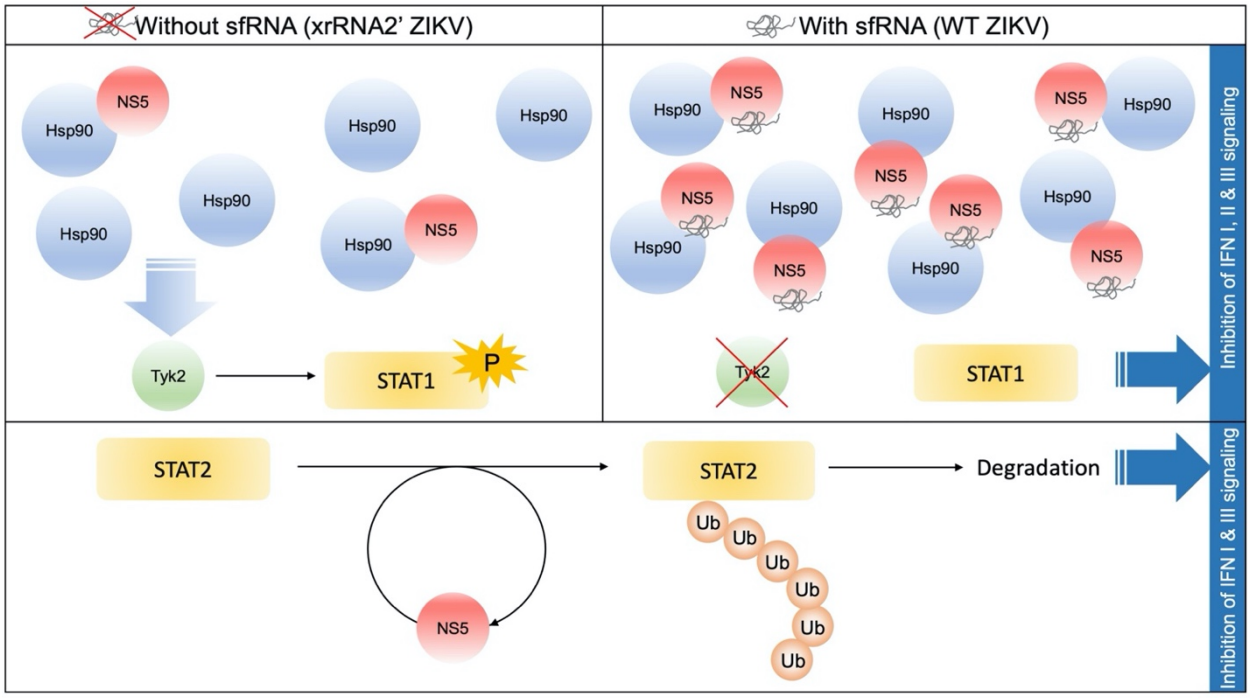

No sfRNA	No NS5	STAT2 activation	STAT1 activation	Strong antiviral response via STAT1/STAT2 and STAT1/STAT1 pathways
No sfRNA	Small amount of NS5	STAT2 degradation	STAT1 activation	Weaker antiviral response – STAT1/STAT1 pathway only
sfRNA production	Stabilisation of NS5 creates large NS5 amount	STAT2 degradation	No STAT1 phosphorylation and activation	Highly inhibited antiviral response – no STAT signal transduction

Fig. S12.

ZIKV NS5 requires sfRNA to inhibit STAT1 phosphorylation but not induce STAT2 degradation. ZIKV NS5 inhibits STAT1 phosphorylation by binding to the chaperone protein Hsp90, which is required for folding of Tyk2 – the upstream kinase of STAT1 in IFN signalling. The binding of NS5 to Hsp90 competes with the binding of Hsp90 to Tyk2, which results in incorrect folding and subsequent proteasomal degradation of Tyk2 thus preventing STAT1 phosphorylation. As this reaction requires NS5 to constantly form a complex with Hsp90, both proteins must be present in cells in stoichiometric concentrations. Therefore, a large quantity of NS5 is needed, which is achieved by NS5 stabilization with bound sfRNA. The binding of NS5 to STAT2 triggers a chain of reactions that results in the ubiquitination and degradation of STAT2. This is an energy-dependent irreversible reaction for which NS5 acts as a catalyst and can be recycled. Hence, a small quantity of NS5 produced in cells infected with a sfRNA-deficient virus is sufficient for STAT2 degradation. In summary, sfRNA facilitates NS5-dependent inhibition of STAT1 phosphorylation leading to inhibition of responses to all 3 types of IFNs to enable initial infection, systemic spread and trans-placental dissemination of ZIKV.

Table S1. (separate file)

Statistical analysis of blood viremia in AG129 mice. Comparison was performed using Student's t-test on areas under the curves (AUC).

Table S2. (separate file)

Statistical analysis of CPE in Fig. 1D.

Table S3. (separate file)

Statistical analysis of viremia in IFNAR-/- dams inoculated with 10^4 FFU ZIKV.

Table S4. (separate file)

Statistical analysis of viremia in IFNAR-/- dams inoculated with 10^6 FFU ZIKV.

Table S5. (separate file)

Comparison of blood viremia between pregnant mice infected with 10^4 FFU WT ZIKV and 10^6 FFU xrRNA1' mutant ZIKV. Comparison was performed using Student's t-test on areas under the curves (AUC).

Table S6. (separate file)

Comparison of blood viremia between pregnant mice infected with 10^4 FFU WT ZIKV and 10^6 FFU xrRNA2' mutant ZIKV.

Table S7. (separate file)

Statistical comparison of WT and mutant ZIKV replication in DIV15 human cerebral organoids.

Table S8. (separate file)

Statistical comparison of WT and mutant ZIKV replication in DIV30 human cerebral organoids.

Table S9. (separate file)

Statistical comparison of gene expression levels in BeWo cell infected with WT ZIKV vs xrRNA2' mutant virus.

Table S10. (separate file)

Upstream regulators for DEGs affected by sfRNA production.

Table S11. (separate file)

Oligonucleotides used in the study

Table S12. (separate file)

Antibodies used for Western blotting.